Stochastic simulation of the partition mechanism under diffusion-limited conditions in chromatography and electrochromatography

Victoria L. McGuffin*, Peter E. Krouskop, Peiru Wu

Department of Chemistry and Center for Fundamental Materials Research, Michigan State University, East Lansing, MI 48824-1322, USA

Abstract

A three-dimensional stochastic simulation has been used to study the kinetics of the partition mechanism in a homogeneous system under diffusion-limited conditions. By nonlinear regression of the simulation data, the rate constants for transport between the fluid and surface phases (k_{fs} and k_{sf}) are determined with $\pm 0.49\%$ average relative standard deviation, and the ratio of the rate constants (k_{fs}/k_{sf}) with $\pm 0.70\%$ average relative standard deviation and $\pm 2.25\%$ average relative error. The results of these simulations are used to elucidate the relationship between the rate constants and the fundamental parameters of the system, including the equilibrium constant (K), the diffusion coefficients (D_f and D_s), and the radius of the fluid and surface phases (R_f and R_s). In addition, the influence of slow kinetics on the solute zone profile is characterized under the conditions of laminar and electroosmotic flow. The mean, variance, and asymmetry of the zone profile are shown to vary systematically with the rate constants, the linear velocity, and the distance travelled. © 1998 Published by Elsevier Science B.V. All rights reserved.

Keywords: Kinetics; Stochastic simulation; Partition mechanism; Rate constants; Computer simulation; Absorption; Non-equilibrium

1. Introduction

In a chromatography or electrochromatography system, molecules that are at the front edge of the solute zone in the fluid phase enter a new, previously unoccupied region of the column. Because there are no solute molecules in the surface phase, reequilibration must occur such that the activity or, more simply, the concentration in each phase is in correspondence with the equilibrium constant. At the rear edge of the zone, the complementary process occurs. Solute molecules in the surface phase are left behind, so that there is an activity or concentration deficiency in the fluid phase that must be reequilibrated. In each of these processes, a finite time is required for solute

molecules to diffuse, dissolve, partition, or adsorb in the proper phase. During this time, the solute zone continues to advance and thereby perpetuates and exacerbates the problem. As a result, the solute zone remains in a continuous state of nonequilibrium.

The importance of nonequilibrium and kinetics in separation science has been recognized since the pioneering work of Giddings [1–5]. A detailed understanding of kinetic effects is necessary to identify and to characterize the rate-limiting processes, so that separation speed can be increased without sacrificing efficiency. This understanding is especially important for condensed-phase separations because of the inherently small diffusion coefficients and slow separation speed. The theoretical methods that have been used to study kinetic effects are of two general types: those based on the mass-balance

*Corresponding author.

approach [6–9] and those based on stochastic theory [9–14]. The classical mass-balance approach is, in general, more useful for interpretive rather than predictive models of the zone profile. Because of the fundamental assumptions of these models, they are only accurate in the long-time limit when the solute zone approaches a symmetric Gaussian profile. In addition, these models often neglect certain contributions to the variance or assume that these contributions are independent and additive. These assumptions are not likely to be valid in the short-time limit or for a system that is far from equilibrium. In contrast, the classical stochastic methods are rigorous but difficult to apply to complex separation mechanisms. They have been utilized for one-, two-, and multiple-site adsorption that is kinetically controlled, but not for diffusion-controlled adsorption or partition mechanisms.

More recently, an ab initio type of stochastic simulation has been developed for chromatography and electrophoresis [15–17]. These simulations are based on the migration of individual molecules by the sequential application of independently defined transport processes (Markov chain). The fundamental equations of motion used to describe these transport processes require few, if any, assumptions that limit their general applicability. Thus, these simulations can provide a powerful and versatile means to examine and characterize complex separation systems.

The goals of the present study are as follows: (1) to perform stochastic simulations of the partition process under diffusion-limited conditions in a system with homogeneous fluid and surface phases and to determine the kinetic rate constants, (2) to elucidate the relationships between the rate constants and the fundamental parameters of the system, including the equilibrium constant for distribution of the solute between the fluid and surface phases, the diffusion coefficient of the solute in each phase, and the radial dimensions of each phase, and (3) to examine the relationship between the rate constants and the solute zone profiles in chromatography and electrochromatography.

2. Computer simulation methods

The stochastic computer simulation is written in

the FORTRAN 90 programming language and optimized for execution on an IBM RS/6000 Model 580 computer. A flowchart for the simulation is shown in Fig. 1. This simulation, which has been described in detail in previous studies [16,17], follows the trajectories of individual molecules in three-dimensional space. The simulation incorporates algorithms for the transport processes of diffusion, convection by laminar and electroosmotic flow, electrophoretic migration, and surface interaction by a partition or adsorption mechanism. The selected processes are applied sequentially to each molecule at each time increment (t) until the total simulation time is reached.

The program allows the molecular zone profile to be examined as the time distribution at specified distances or, correspondingly, as the distance distribution at specified times. The zone profile is then characterized by means of the statistical moments. For example, the first statistical moment ($M1$) or mean retention time is calculated as
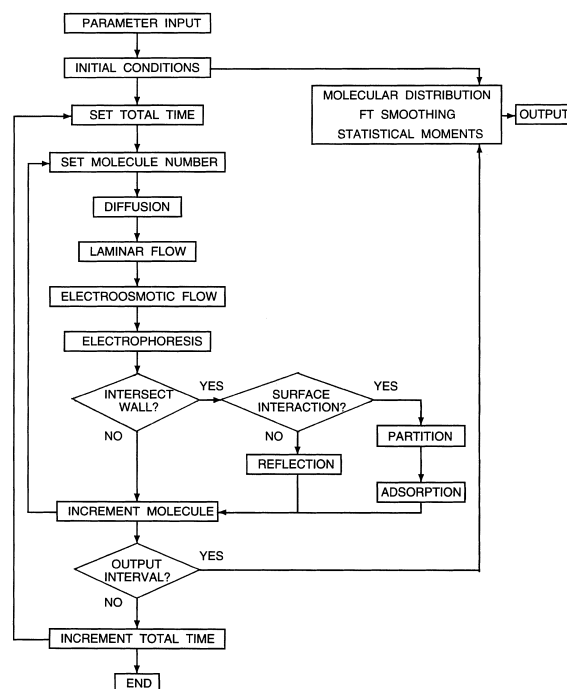
$$M1 = N^{-1} \sum_{i=1}^{N} T_i \tag{1}$$

Fig. 1. Flowchart of the stochastic simulation program.

the second statistical moment ($M2$) or variance is calculated as

$$M2 = N^{-1} \sum_{i=1}^{N} (T_i - M1)^2 \tag{2}$$

and the third statistical moment ($M3$) or asymmetry is calculated as

$$M3 = N^{-1} \sum_{i=1}^{N} (T_i - M1)^3 \tag{3}$$

where T_i is the arrival time of an individual molecule at the specified distance and N is the total number of molecules. These statistical moments, as well as the chromatographic or electrophoretic figures of merit derived therefrom, are stored in a standard data file at each specified distance (or time). In addition to the numerical output parameters, the molecular population is summed in discrete segments of time (or length) and then smoothed by Fourier transform methods [18] to provide a continuous zone profile for graphical display.

The stochastic simulation has been fully validated over the range of conditions commonly encountered in gas, supercritical fluid, and liquid chromatography [16] as well as electrophoresis [17]. In the present study, this simulation is applied to characterize solute transport during the partition process under diffusion-limited conditions. The model system consists of a homogeneous fluid phase with radius R_f in contact with a permeable, homogeneous surface phase with radial depth R_s. The solute has diffusion coefficients D_f and D_s in the fluid and surface phases, respectively, and is distributed between these phases with an equilibrium constant K. This model system is used to simulate chromatography and electrochromatography separations in open-tubular columns.

3. Results and discussion

In the partition process, the solute X is distributed between the fluid (f) and surface (s) phases:

$$X_f \underset{k_{sf}}{\overset{k_{fs}}{\rightleftarrows}} X_s \tag{4}$$

where k_{fs} and k_{sf} are the pseudo-first-order rate constants. Under these conditions, the distribution of solute molecules can be described by a simple kinetic model of reversible reactions [19,20]. The net rate of change in the number of molecules in the fluid and surface phases (N_f and N_s, respectively) is governed by the following system of ordinary differential equations:

$$\frac{dN_f}{dT} = -k_{fs}N_f + k_{sf}N_s \tag{5a}$$

$$\frac{dN_s}{dT} = k_{fs}N_f - k_{sf}N_s \tag{5b}$$

If all molecules initially reside in the fluid phase, then the solution of Eqs. (5a) and (5b) is given by

$$\frac{N_f}{N} = \frac{k_{sf} + k_{fs}\exp(-(k_{fs} + k_{sf})T)}{(k_{fs} + k_{sf})} \tag{6a}$$

$$\frac{N_s}{N} = \frac{k_{fs} - k_{fs}\exp(-(k_{fs} + k_{sf})T)}{(k_{fs} + k_{sf})} \tag{6b}$$

From Eqs. (6a) and (6b), it follows directly that

$$\tilde{N}_f = \lim_{T \to \infty} N_f = \frac{k_{sf}N}{(k_{fs} + k_{sf})} \tag{7a}$$

$$\tilde{N}_s = \lim_{T \to \infty} N_s = \frac{k_{fs}N}{(k_{fs} + k_{sf})} \tag{7b}$$

where $\tilde{N}_f$ and $\tilde{N}_s$ represent the number of molecules in the fluid and surface phases at equilibrium. Hence, the ratio of the number of molecules $\tilde{N}_s/\tilde{N}_f$ under the equilibrium definition is equal to the ratio of the rate constants k_{fs}/k_{sf} under the kinetic definition:

$$\frac{\tilde{N}_s}{\tilde{N}_f} = \frac{k_{fs}}{k_{sf}} = k = \frac{KV_s}{V_f} \tag{8}$$

Furthermore, this ratio defines the capacity factor (k), which represents the equilibrium constant (K) adjusted for the volumes of the fluid and surface phases (V_f and V_s, respectively). For the cylindrical model system, these volumes are given by

$$V_f = \pi R_f^2 L \tag{9a}$$

$$V_s = \pi[(R_f + R_s)^2 - R_f^2]L = \pi(R_s^2 + 2R_fR_s)L \tag{9b}$$

To examine the kinetic and equilibrium behavior of the model system, the number of molecules in the fluid phase is monitored as a function of time during the stochastic simulation. Three to five repetitive

simulations with 10 000 molecules are averaged to obtain the simulation data $(T, N_f/N)$. The kinetic rate constants are then determined by nonlinear regression of the simulation data to Eq. (6a), as illustrated in Fig. 2. In addition, the ratio of the number of molecules $\tilde{N}_s/\tilde{N}_f$ is calculated after equilibrium has been attained [21].

3.1. Effect of parameters on equilibrium processes

As noted above, the ratio of the number of molecules in the fluid and surface phases $\tilde{N}_s/\tilde{N}_f$ reflects the equilibrium behavior of the system. This ratio was determined by stochastic simulation as a function of the equilibrium constant (Table 1), the diffusion coefficients in the fluid and surface phases (Table 2), and the radial depth of the fluid and surface phases (Table 3). The theoretically expected relationship between the $\tilde{N}_s/\tilde{N}_f$ ratio and these parameters is given in Eqs. (8) and (9). The simulation data show excellent agreement with this theoretical relationship, as verified in Fig. 3. The $\tilde{N}_s/\tilde{N}_f$ ratio is determined with ±0.29% average relative standard deviation and ±0.39% average relative error.
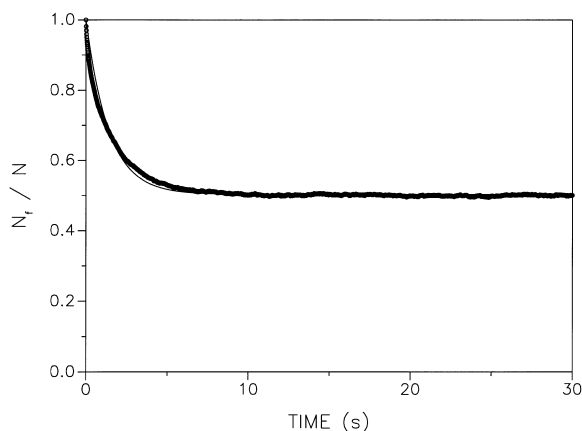

Fig. 2. Kinetic evolution of the partition process by monitoring the relative number of molecules in the fluid phase (N_f/N) as a function of simulation time (T). Simulation conditions: $N =$ 10 000, $t = 5.0 \times 10^{-4}$ s, $K = 1.0$, $D_f = 1.0 \times 10^{-5}$ cm^2 s^{-1}, $D_s = 1.0 \times 10^{-7}$ cm^2 s^{-1}, $R_f = 2.00 \times 10^{-3}$ cm, $R_s = 8.28 \times 10^{-4}$ cm. (—-) Nonlinear regression analysis according to Eq. (6a), yielding rate constants $k_{fs} = 0.353 \pm 0.001$, $k_{sf} = 0.357 \pm 0.001$ ($r^2 = 0.974$).

Table 1
Kinetic rate constants k_{fs} and k_{sf} determined by nonlinear regression of the simulation data to Eq. (6a)

K	k_{fs} (s^{-1})	k_{sf} (s^{-1})	k_{fs}/k_{sf}	$\tilde{N}_s/\tilde{N}_f$
0.1	2.765±0.011	27.78±0.112	0.100	0.100
0.2	4.988±0.017	25.00±0.090	0.200	0.200
0.5	9.495±0.041	19.10±0.086	0.497	0.504
1.0	13.74±0.069	13.87±0.074	0.991	0.999
2.0	16.43±0.078	8.363±0.044	1.965	1.992
5.0	17.95±0.081	3.713±0.022	4.836	4.954
10.0	18.37±0.083	1.971±0.016	9.323	9.924

Simulation conditions: $N = 10\,000$, $t = 5.0 \times 10^{-4}$ s, $K =$ variable, $D_f = 1.0 \times 10^{-5}$ cm^2 s^{-1}, $D_s = 1.0 \times 10^{-5}$ cm^2 s^{-1}, $R_f = 2.00 \times 10^{-3}$ cm, $R_s = 8.28 \times 10^{-4}$ cm.

3.2. Effect of parameters on kinetic processes

The kinetic rate constants k_{fs} and k_{sf} were also determined as a function of the equilibrium constant (Table 1), the diffusion coefficients in the fluid and surface phases (Table 2), and the radial depth of the fluid and surface phases (Table 3). The theoretically expected relationship between the ratio of the rate constants k_{fs}/k_{sf} and these parameters is given in Eqs. (8) and (9). The simulation data show excellent agreement with this theoretical relationship, as verified in Fig. 4. The individual rate constants k_{fs} and k_{sf} are determined with ±0.49% average relative standard deviation, and the ratio of the rate constants k_{fs}/k_{sf} with ±0.70% average relative standard deviation and ±2.25% average relative error.

Although the ratio of the rate constants k_{fs}/k_{sf} can be readily predicted by Eq. (8), there is no theoretical model presently available to determine the magnitude of the individual rate constants k_{fs} and k_{sf}. For this reason, the stochastic simulation approach has been used to elucidate the relationships between the diffusion-limited rate constants and the fundamental parameters of the system.

The equilibrium constant was varied from 0.1 to 10.0, with all other parameters remaining constant. The effect of the variation in equilibrium constant on the individual rate constants is summarized in Table 1. It is apparent that k_{fs} increases nonlinearly whereas k_{sf} decreases nonlinearly with an increase in equilibrium constant. Upon detailed examination, the following relationships appear to be applicable:

Table 2
Kinetic rate constants k_{fs} and k_{sf} determined by nonlinear regression of the simulation data to Eq. (6a)

D_f (cm^2 s^{-1})	D_s (cm^2 s^{-1})	k_{fs} (s^{-1})	k_{sf} (s^{-1})	k_{fs}/k_{sf}	$\tilde{N}_s/\tilde{N}_f$
1.0×10^{-4}	1.0×10^{-5}	30.94 ± 0.09	31.25 ± 0.10	0.990	1.008
1.0×10^{-4}	1.0×10^{-6}	3.635 ± 0.016	3.690 ± 0.017	0.985	0.988
1.0×10^{-4}	1.0×10^{-7}	0.366 ± 0.001	0.363 ± 0.002	1.009	1.023
1.0×10^{-5}	1.0×10^{-4}	21.49 ± 0.097	21.95 ± 0.106	0.979	1.000
1.0×10^{-5}	1.0×10^{-5}	13.74 ± 0.069	13.87 ± 0.074	0.991	0.999
1.0×10^{-5}	1.0×10^{-6}	3.076 ± 0.010	3.102 ± 0.011	0.991	1.006
1.0×10^{-5}	1.0×10^{-7}	0.353 ± 0.001	0.357 ± 0.001	0.989	0.999
1.0×10^{-5}	1.0×10^{-8}	0.0380 ± 0.0002	0.0386 ± 0.0002	0.986	0.999
1.0×10^{-5}	1.0×10^{-9}	0.00388 ± 0.00001	0.00377 ± 0.00001	1.027	1.020
1.0×10^{-5}	1.0×10^{-10}	0.00040 ± 0.000001	0.00041 ± 0.000001	0.982	0.951
1.0×10^{-6}	1.0×10^{-4}	2.199 ± 0.011	2.238 ± 0.012	0.983	0.988
1.0×10^{-6}	1.0×10^{-5}	2.204 ± 0.011	2.265 ± 0.012	0.973	1.001
1.0×10^{-6}	1.0×10^{-6}	1.381 ± 0.004	1.391 ± 0.004	0.993	1.008
1.0×10^{-6}	1.0×10^{-7}	0.308 ± 0.001	0.306 ± 0.001	1.006	0.979
1.0×10^{-6}	1.0×10^{-8}	0.0370 ± 0.0001	0.0381 ± 0.0001	0.972	1.001
1.0×10^{-7}	1.0×10^{-5}	0.233 ± 0.001	0.240 ± 0.001	0.972	1.001
1.0×10^{-7}	1.0×10^{-6}	0.221 ± 0.001	0.225 ± 0.001	0.982	0.976

Simulation conditions: $N=10\,000$, $t=5.0\times10^{-4}$ s, $K=1.0$, D_f=variable, D_s=variable, $R_f=2.00\times10^{-3}$ cm, $R_s=8.28\times10^{-4}$ cm.

$$k_{fs}\propto\left(\frac{K}{1+K}\right) \tag{10a}$$

$$k_{sf}\propto\left(\frac{1}{1+K}\right) \tag{10b}$$

These relationships suggest that the rate constant for transport from the fluid to surface phase is controlled by the fraction of molecules in the surface phase at equilibrium and, conversely, the rate constant for transport from the surface to fluid phase is dictated by the fraction of molecules in the fluid phase at equilibrium.

The diffusion coefficient in the fluid phase was

Table 3
Kinetic rate constants k_{fs} and k_{sf} determined by nonlinear regression of the simulation data to Eq. (6a)

R_f (cm)	R_s (cm)	k_{fs} (s^{-1})	k_{sf} (s^{-1})	k_{fs}/k_{sf}	$\tilde{N}_s/\tilde{N}_f$
1.13×10^{-3}	8.28×10^{-4}	32.90 ± 0.088	16.59 ± 0.050	1.983	2.008
2.00×10^{-3}	8.28×10^{-4}	13.74 ± 0.069	13.87 ± 0.074	0.991	0.999
3.69×10^{-3}	8.28×10^{-4}	5.279 ± 0.026	10.72 ± 0.055	0.492	0.500
8.68×10^{-3}	8.28×10^{-4}	1.615 ± 0.014	8.332 ± 0.076	0.194	0.200
1.70×10^{-2}	8.28×10^{-4}	0.721 ± 0.006	7.686 ± 0.069	0.094	0.098
3.35×10^{-2}	8.28×10^{-4}	0.337 ± 0.003	7.186 ± 0.063	0.047	0.049
8.33×10^{-2}	8.28×10^{-4}	0.128 ± 0.001	6.811 ± 0.059	0.019	0.020
2.00×10^{-3}	9.76×10^{-5}	52.27 ± 0.40	533.8 ± 4.4	0.094	0.098
2.00×10^{-3}	1.91×10^{-4}	28.49 ± 0.18	144.9 ± 0.95	0.197	0.199
2.00×10^{-3}	4.49×10^{-4}	18.03 ± 0.079	36.69 ± 0.17	0.491	0.498
2.00×10^{-3}	1.46×10^{-3}	10.69 ± 0.036	5.410 ± 0.020	1.977	1.980
2.00×10^{-3}	2.90×10^{-3}	7.753 ± 0.029	1.587 ± 0.007	4.885	4.960
2.00×10^{-3}	4.63×10^{-3}	6.469 ± 0.030	0.718 ± 0.005	9.014	10.028

Simulation conditions: $N=10\,000$, $t=5.0\times10^{-4}$ s, $K=1.0$, $D_f=1.0\times10^{-5}$ cm^2 s^{-1}, $D_s=1.0\times10^{-5}$ cm^2 s^{-1}, R_f=variable, R_s=variable.
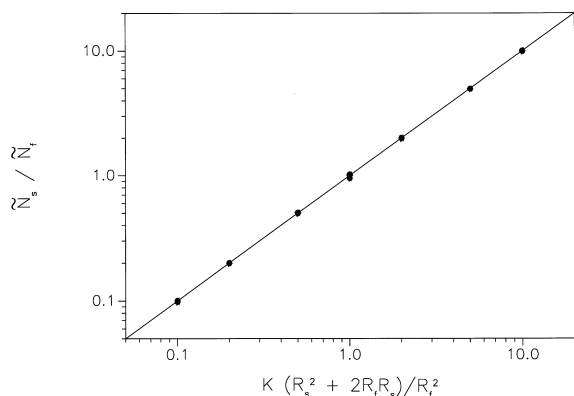
Fig. 3. Relationship between the ratio of molecules in the fluid and surface phases at equilibrium ($\bar{N}_s/\bar{N}_f$) and the equilibrium constant (K) and the radius of the fluid and surface phases (R_f and R_s, respectively). (—) Theory according to Eqs. (8) and (9) ($r^2 =$ 1.000). Simulation conditions given in Tables 1–3.

varied from 10^{-4} to 10^{-7} cm^2 s^{-1} and the diffusion coefficient in the surface phase was varied from 10^{-4} to 10^{-10} cm^2 s^{-1}, with all other parameters remaining constant. The effect of the variation in diffusion coefficient on the individual rate constants is summarized in Table 2. It is apparent that both k_{fs} and k_{sf} increase with an increase in the diffusion coefficients in the fluid and surface phases. Upon detailed examination, the following relationships are elucidated:
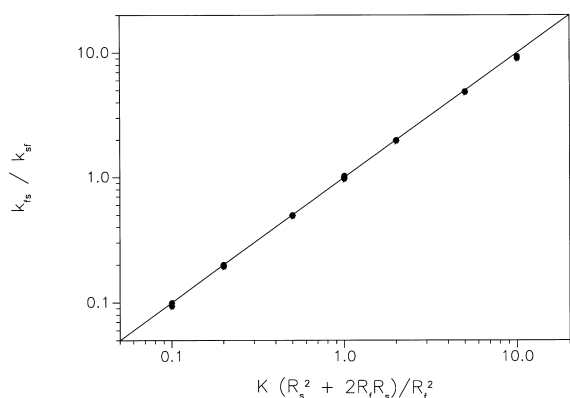
Fig. 4. Relationship between the ratio of the rate constants (k_{fs}/k_{sf}) and the equilibrium constant (K) and the radius of the fluid and surface phases (R_f and R_s, respectively). (—) Theory according to Eqs. (8) and (9) ($r^2 = 0.999$). Simulation conditions given in Tables 1–3.

$$k_{fs} \propto \left(\frac{1}{D_f} + \frac{1}{D_s} \right)^{-1} \tag{11a}$$

$$k_{sf} \propto \left(\frac{1}{D_f} + \frac{1}{D_s} \right)^{-1} \tag{11b}$$

These relationships indicate that the rate constants are controlled by the reduced diffusion coefficient of the system. When the diffusion coefficients in the fluid and surface phases are of comparable magnitude, both have a manifest influence upon the rate constants. However, when one diffusion coefficient is notably smaller than the other, it serves to limit the overall transport rate.

The radius of the fluid phase was varied from 1.13×10^{-3} to 8.33×10^{-2} cm and the radius of the surface phase was varied from 9.76×10^{-5} to 4.63×10^{-3} cm, with all other parameters remaining constant. These radii result in a volume ratio of the fluid and surface phases (V_f/V_s) ranging from 0.1 to 50.0. The effect of the variation in radius on the individual rate constants is summarized in Table 3. Both k_{fs} and k_{sf} decrease in a complex manner with an increase in the radius of either the fluid or surface phase. The following relationships appear to be applicable:

$$k_{fs} \propto \left(\frac{2R_f R_s + R_s^2}{R_f^2 + 2R_f R_s + R_s^2} \right) \left(\frac{(R_f + \pi R_s)^2}{(\pi R_f + \pi R_s)^{0.5} R_f^{1.5} R_s^2} \right) \tag{12a}$$

$$k_{sf} \propto \left(\frac{R_f^2}{R_f^2 + 2R_f R_s + R_s^2} \right) \left(\frac{(R_f + \pi R_s)^2}{(\pi R_f + \pi R_s)^{0.5} R_f^{1.5} R_s^2} \right) \tag{12b}$$

These relationships suggest that there are two important radius-dependent contributions, one of which is common and the other specific to the individual rate constants. The specific contribution, shown in the left-hand term of Eqs. (12a) and (12b), indicates that the rate of transport from fluid to surface phase depends on the volume ratio of the surface phase to the total system. Conversely, the rate of transport from surface to fluid phase depends on the volume ratio of the fluid phase to the total system. The common contribution, shown in the right-hand term of Eqs. (12a) and (12b), suggests that the radii of the fluid and surface phases operate in a concerted manner if they are of comparable magnitude. How-

ever, if one radius is notably larger than the other, it predominantly controls the overall transport rate.

Upon appropriate combination of Eqs. (10a), (10b), (11a), (11b), (12a), (12b), the following expressions for the rate constants are obtained:

$$k_{fs} = \left(\frac{K(2R_f R_s + R_s^2)}{R_f^2 + K(2R_f R_s + R_s^2)} \right) \left(\frac{1}{D_f} + \frac{1}{D_s} \right)^{-0.5}$$

$$\times \left(\frac{\pi R_f}{D_f} + \frac{\pi R_s}{D_s} \right)^{-0.5} \left(\frac{(R_f + \pi R_s)^2}{R_f^{1.5} R_s^2} \right) \qquad (13a)$$

$$k_{sf} = \left(\frac{R_f^2}{R_f^2 + K(2R_f R_s + R_s^2)} \right) \left(\frac{1}{D_f} + \frac{1}{D_s} \right)^{-0.5}$$

$$\times \left(\frac{\pi R_f}{D_f} + \frac{\pi R_s}{D_s} \right)^{-0.5} \left(\frac{(R_f + \pi R_s)^2}{R_f^{1.5} R_s^2} \right) \qquad (13b)$$

These equations indicate that the term involving the equilibrium constant in Eqs. (10a) and (10b) is coupled with that for the volume of the fluid and surface phases in Eqs. (12a) and (12b). This coupling is intuitively meaningful, since the capacity factor in Eq. (8) is defined by this relationship. In addition, the reduced diffusion coefficient in Eqs. (11a) and (11b) is coupled, in part, to the reduced radius in Eqs. (12a) and (12b). This coupling is also meaningful, since it denotes the rate of diffusion relative to the distance over which that diffusion occurs. Fig. 5A and B demonstrate the excellent agreement obtained between the rate constants determined by the stochastic simulation and those predicted by Eqs. (13a) and (13b) over the entire range of parameters given in Tables 1–3. From linear regression analysis of k_{fs} and k_{sf} according to Eqs. (13a) and (13b), the slopes are 1.01 and 1.11, respectively, the intercepts are -0.02 and -0.60, respectively, and the square of the linear correlation coefficients (r^2) are 0.989 and 0.999, respectively. Because the slopes appear to be nearly unity and the intercepts appear to be nearly zero, this suggests that all important parameters have been considered. In addition, the ratio of the rate constants k_{fs}/k_{sf} evaluated by using Eqs. (13a) and (13b) is equivalent to $K V_s/V_f$, as given by Eqs. (8) and (9). Thus, we may conclude that the relationships for the rate constants in a homogeneous fluid and surface phase under diffusion-limited conditions have been fully resolved. The individual rate con-
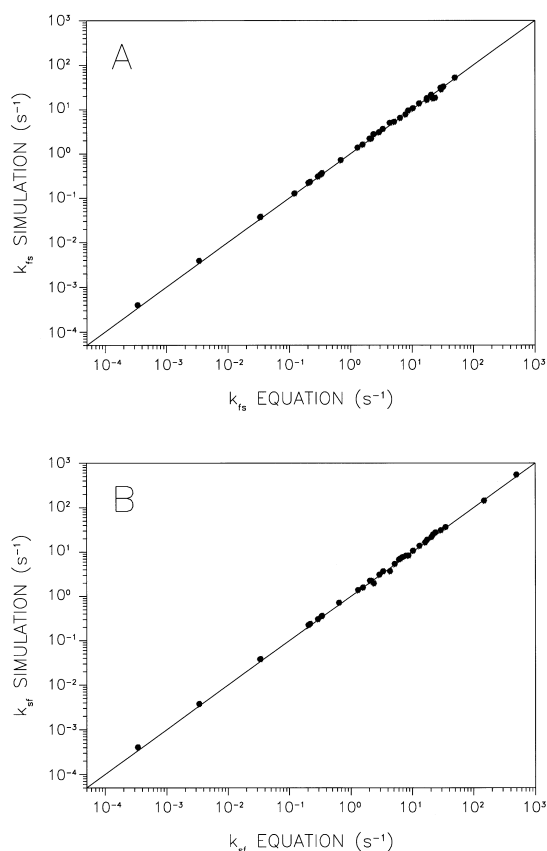

Fig. 5. Relationship between the individual rate constants k_{fs} and k_{sf} determined by stochastic simulation and predicted by Eqs. (13a) and (13b). Simulation conditions given in Tables 1–3.

stants k_{fs} and k_{sf} can be predicted by using Eqs. (13a) and (13b) with average relative errors of $\pm 4.36\%$ and $\pm 6.59\%$, respectively, in the range from 10^{-3} to 10^3 s^{-1}.

The overall kinetic behavior of the system can be described in terms of the characteristic time τ. This represents the time required for the number of molecules in the fluid phase N_f/N to reach $1 - (1/e)$ of the number at equilibrium $\tilde{N}_f/N$. For the reversible pseudo-first-order system in Eq. (4), the characteristic time is given by

$$\tau = \left(\frac{1}{k_{fs} + k_{sf}} \right) \qquad (14)$$

which can be readily evaluated by substitution of k_{fs} and k_{sf} from Eqs. (13a) and (13b).

Finally, it is desirable to evaluate the sensitivity of the rate constants k_{fs} and k_{sf} as well as the characteristic time τ to changes in the various parameters. This can be easily achieved by calculating the partial derivatives of Eqs. (13) and (14), e.g. $\partial k_{fs}/\partial K$, $\partial k_{sf}/\partial K$, $\partial \tau/\partial K$, etc., as summarized in the Appendix. It is noteworthy that the derivatives of the rate constants k_{fs} and k_{sf} with respect to the equilibrium constant K are opposite in sign. These contributions balance such that the characteristic time τ is independent of K. The derivatives of both rate constants with respect to the diffusion coefficients D_f and D_s are positive, leading to a strong negative dependence of the characteristic time τ. Finally, the derivatives of both rate constants with respect to the radii R_f and R_s are negative, leading to a strong positive dependence of the characteristic time τ. These conclusions are in accord with the general trends observed in Tables 1–3.

3.3. Effect of kinetic rate constants on zone profiles in chromatography and electrochromatography

In the presence of convective flow, the characteristic time τ will influence the appearance of the solute zone profiles. If τ is sufficiently small, the system will be nearly at equilibrium and the zone profile will be a symmetric Gaussian distribution. Under these conditions, the profile will be well described by the classical equations of mass balance using the equilibrium-dispersive model [6–9]. As τ increases, however, the system may depart from equilibrium and the zone profile may become highly asymmetric. As a measure of the degree of departure from equilibrium for convective systems, we may define a unitless kinetic parameter P as

$$P = \frac{\tau}{T} = \frac{\tau v}{d} \tag{15}$$

where T is time, d is distance, and v is the linear velocity. This parameter directly reflects the sources of kinetic stress that are placed on the system and will approach a limiting value of zero for a system that is at equilibrium. It is apparent from this definition that kinetic stress arises from the characteristic time τ as well as the linear velocity and the distance travelled.

In order to examine the influence of each of these sources of kinetic stress, a standard system has been selected for stochastic simulation. For a solute with an equilibrium constant $K=1.0$, diffusion coefficients $D_f = 1.0 \times 10^{-5}$ cm^2 s^{-1} and $D_s = 1.0 \times 10^{-7}$ cm^2 s^{-1}, and radii $R_f = 2.00 \times 10^{-3}$ cm and $R_s = 8.28 \times 10^{-4}$ cm, the characteristic time τ shown graphically in Fig. 2 is 1.408 s. The evolution of the corresponding solute zone profile for this system is shown as a function of distance travelled in Fig. 6A for laminar flow at a fixed linear velocity of 0.1 cm s^{-1}. The initial profile, which is obtained at a distance of 0.1 cm ($P = \tau = 1.408$), appears to be highly asymmetric. The degree of asymmetry gradually decreases as the solute zone travels distances of
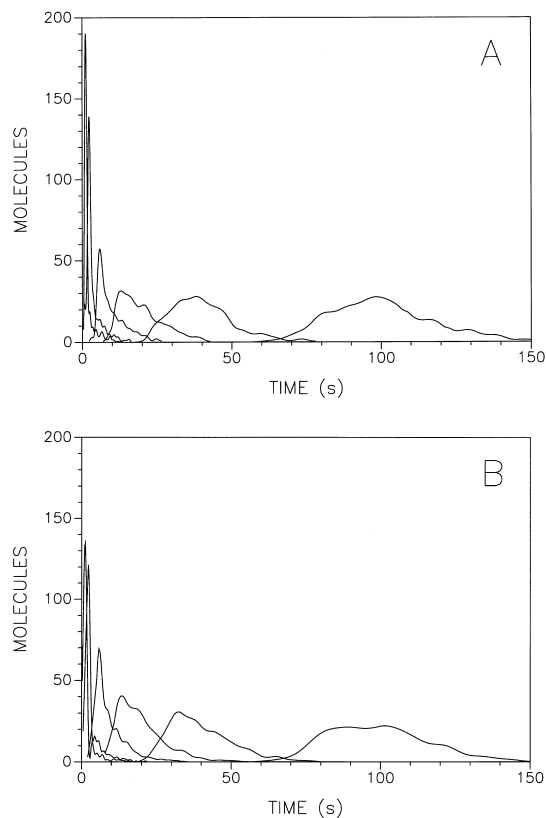

Fig. 6. Evolution of the solute zone profile as a function of distance with laminar flow (A) and electroosmotic flow (B). Simulation conditions: $N=1000$, $t=5.0 \times 10^{-5}$ s, $K=1.0$, $D_f = 1.0 \times 10^{-5}$ cm^2 s^{-1}, $D_s = 1.0 \times 10^{-7}$ cm^2 s^{-1}, $R_f = 2.00 \times 10^{-3}$ cm, $R_s = 8.28 \times 10^{-4}$ cm, $v = 0.1$ cm s^{-1}, $d = 0.1, 0.2, 0.5, 1.0, 2.0, 5.0$ cm.

0.2 cm ($P = \tau/2 = 0.704$), 0.5 cm ($P = \tau/5 = 0.282$), 1.0 cm ($P = \tau/10 = 0.141$), and 2.0 cm ($P = \tau/20 = 0.070$). At the final distance of 5.0 cm ($P = \tau/50 = 0.028$), there is only a slight appearance of asymmetry. The evolution of the solute zone profile is shown in Fig. 6B for electroosmotic flow at a fixed linear velocity of 0.1 cm s^{-1}. Again, the degree of asymmetry is high in the initial profile and gradually decreases until it is only slightly apparent in the final profile. The statistical moments of these zone profiles are calculated by means of Eqs. (1) to (3) and are shown as a function of distance travelled in Fig. 7. The first statistical moment, which represents the mean retention time, increases in the theoretically expected linear manner with distance. The second and third statistical moments, which represent the variance and asymmetry, also increase linearly with distance. The skew of the zone profile, represented by the Gram–Charlier series as $M3/(M2)^{3/2}$ [22,23],

must therefore decrease with the square root of distance. In other words, the solute zone becomes broader but more symmetric as it traverses the chromatography or electrochromatography system. It is noteworthy that the profiles with laminar flow are not visibly broader or less symmetric than those with electroosmotic flow (*vide infra*).

The effect of the linear velocity has been examined at a fixed distance of 5.0 cm and a fixed characteristic time τ for the standard system described above. As shown in Fig. 8, the solute zone profile becomes increasingly asymmetric as the linear velocity is increased from 0.1 cm s^{-1} ($P = \tau/50 = 0.028$) to 1.0 cm s^{-1} ($P = \tau/5 = 0.282$). These zone profiles are characterized by means of the statistical moments in Fig. 9 for both laminar and electroosmotic flow. The first moment varies in the theoretically expected inverse manner with velocity. The second and third moments also vary inversely
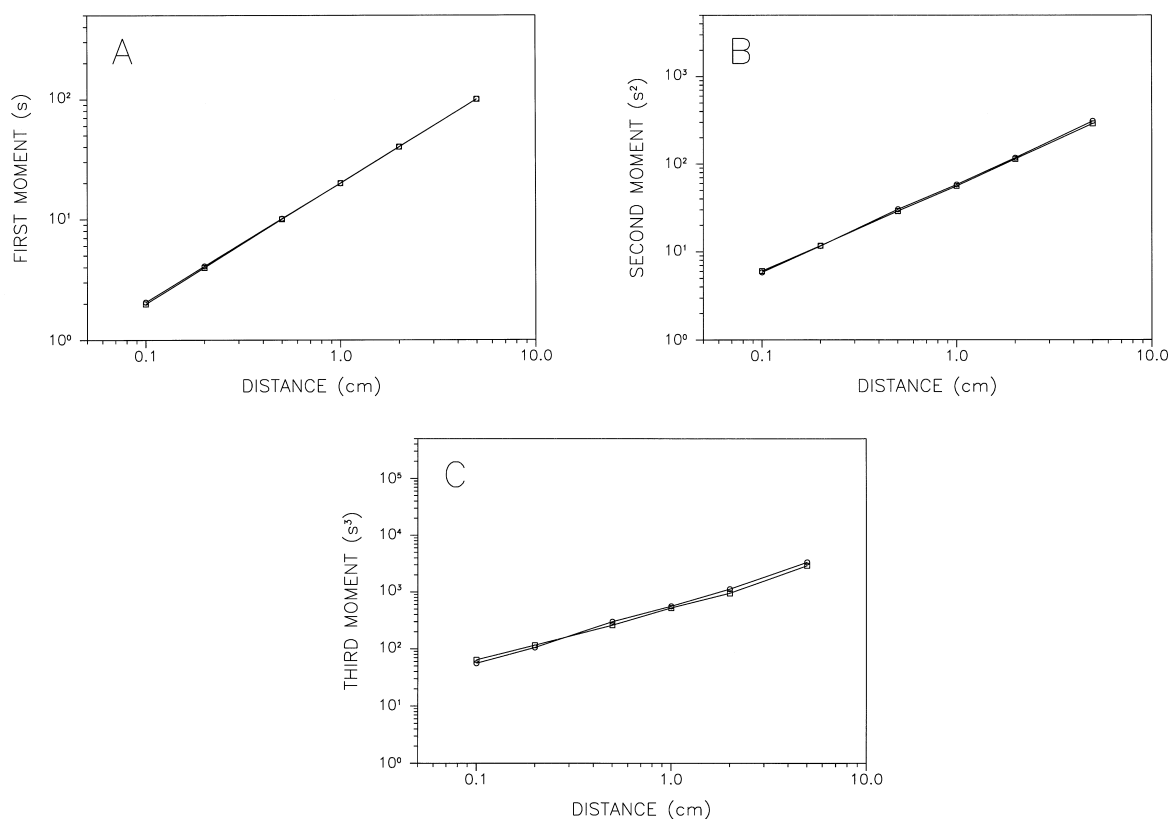

Fig. 7. First (A), second (B), and third (C) statistical moments of the solute zone profiles as a function of the distance travelled for laminar flow (○) and electroosmotic flow (□). Simulation conditions given in Fig. 6.
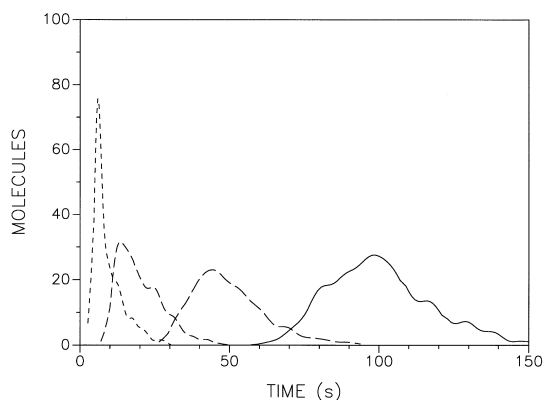
Fig. 8. Solute zone profile as a function of the linear velocity of laminar flow. Simulation conditions: $N = 1000$, $t = 5.0 \times 10^{-5}$ s, $K = 1.0$, $D_f = 1.0 \times 10^{-5}$ cm^2 s^{-1}, $D_s = 1.0 \times 10^{-7}$ cm^2 s^{-1}, $R_f = 2.00 \times 10^{-3}$ cm, $R_s = 8.28 \times 10^{-4}$ cm, $v = 0.1$ cm s^{-1} (——), 0.2 cm s^{-1} (— — —), 0.5 cm s^{-1} (– – –), 1.0 cm s^{-1} (- - -), $d = 5.0$ cm.

with velocity. Consequently, the skew $M3/(M2)^{3/2}$ must increase with the square root of the velocity. In other words, the solute zone becomes less broad but more skewed as the linear velocity increases.

The effect of the characteristic time τ has been examined at a fixed linear velocity of 0.1 cm s^{-1} and a fixed distance of 5.0 cm. Although any of the parameters in Eqs. (13a) and (13b) may be used, we have chosen to vary the parameter that has the greatest influence upon τ. By evaluation of the partial derivatives given in the Appendix under the conditions of the standard system, $\partial \tau / \partial K = 0$, $\partial \tau / \partial D_f = -2.5 \times 10^3$, $\partial \tau / \partial D_s = -1.5 \times 10^7$, $\partial \tau / \partial R_f = 4.8 \times 10^2$, and $\partial \tau / \partial R_s = 6.0 \times 10^3$. From this analysis, it is apparent that the diffusion coefficient in the surface phase has the most significant effect. As shown in Fig. 10, the solute zone profile is symmetric for diffusion coefficients of 1.0×10^{-5} cm^2 s^{-1} ($P =$
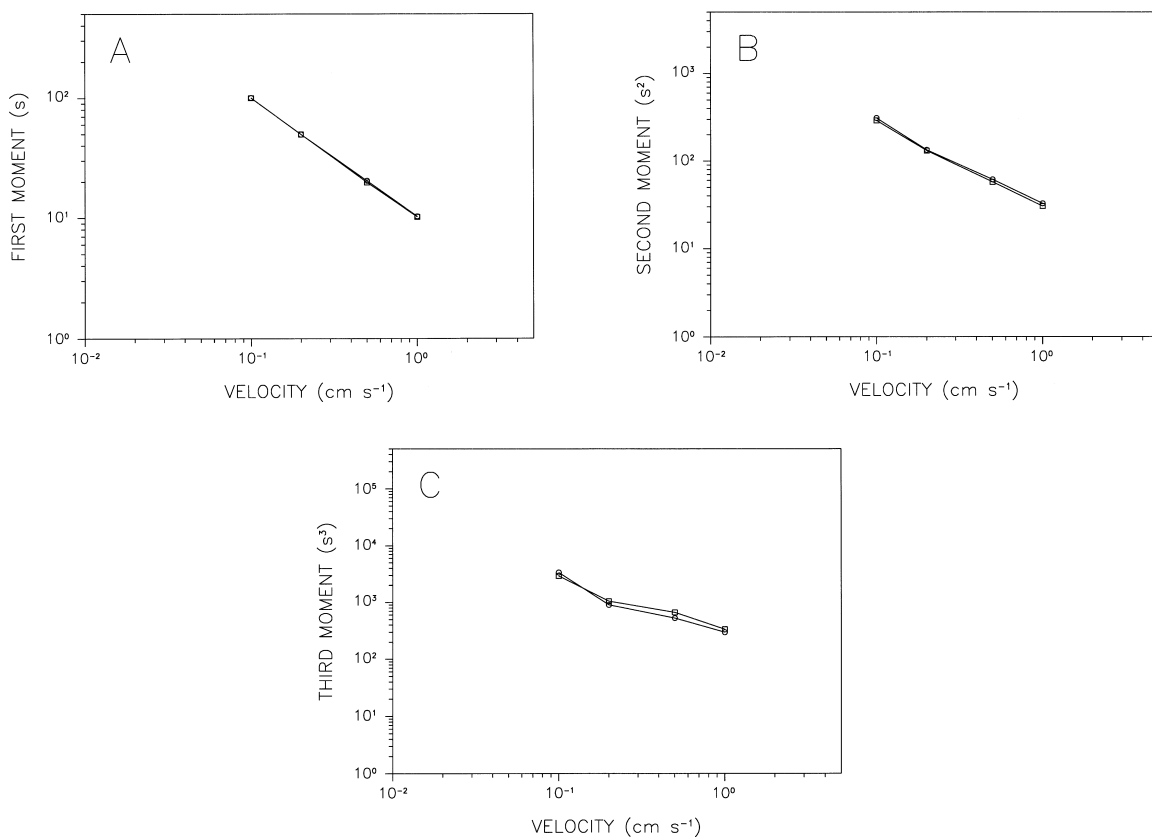

Fig. 9. First (A), second (B), and third (C) statistical moments of the solute zone profiles as a function of the linear velocity for laminar flow (○) and electroosmotic flow (□). Simulation conditions given in Fig. 8.
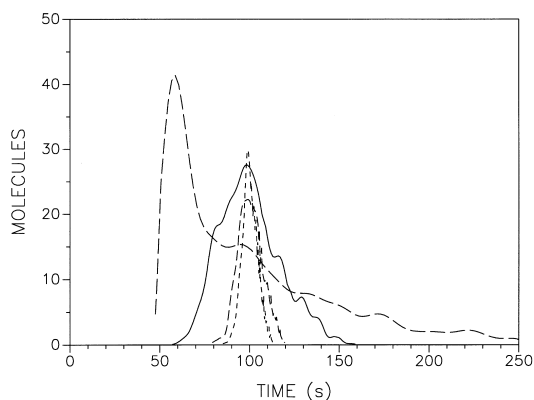
Fig. 10. Solute zone profile as a function of the diffusion coefficient in the surface phase. Simulation conditions: $N=1000$, $t=5.0\times10^{-5}$ s, $K=1.0$, $D_f=1.0\times10^{-5}$ cm^2 s^{-1}, $D_s=1.0\times10^{-5}$ cm^2 s^{-1} (- - -), 1.0×10^{-6} cm^2 s^{-1} (– – –), 1.0×10^{-7} cm^2 s^{-1} (—), 1.0×10^{-8} cm^2 s^{-1} (— — —), $R_f=2.00\times10^{-3}$ cm, $R_s=8.28\times10^{-4}$ cm, $v=0.1$ cm s^{-1}, $d=5.0$ cm.

0.0007) and 1.0×10^{-6} cm^2 s^{-1} ($P=0.003$), becomes slightly asymmetric for 1.0×10^{-7} cm^2 s^{-1} ($P=0.028$), and highly asymmetric for 1.0×10^{-8} cm^2 s^{-1} ($P=0.261$). These zone profiles are characterized by means of the statistical moments in Fig. 11 for both laminar and electroosmotic flow. The first moment is independent of the characteristic time τ. The second moment increases linearly with τ and the third moment increases with the square of τ. Consequently, the skew $M3/(M2)^{3/2}$ must increase with the square root of τ. Thus, the solute zone will become broader and more skewed as the characteristic time τ increases and will have the relationships given in Eqs. (13a) and (13b) to the parameters of the system.

As noted previously, the solute zone profiles with laminar and electroosmotic flow are indistinguishable at higher values of τ (Fig. 11). At the lowest value of
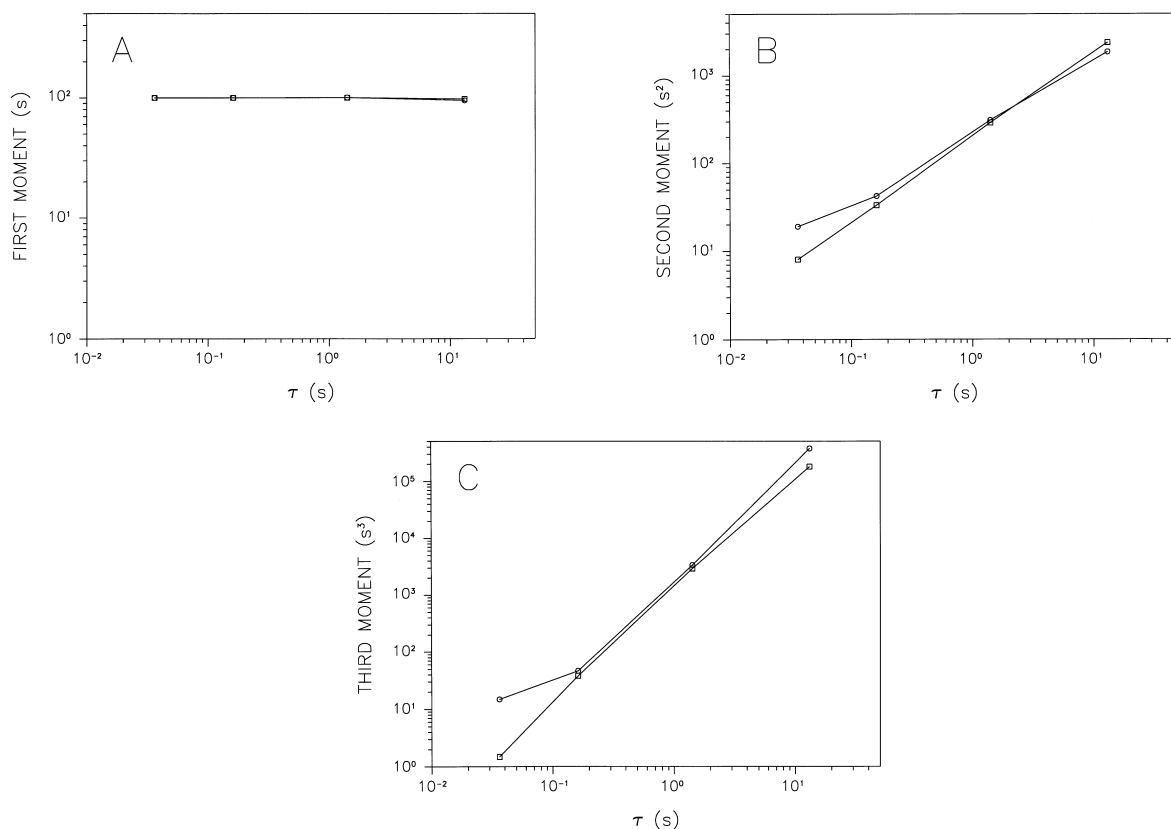

Fig. 11. First (A), second (B), and third (C) statistical moments of the solute zone profiles as a function of the characteristic time τ for laminar flow (○) and electroosmotic flow (□). Simulation conditions given in Fig. 10.

τ, however, the radial flow profile begins to have a manifest influence. The parabolic flow profile characteristic of laminar flow causes a greater increase in variance and asymmetry than the nearly flat flow profile of electroosmotic flow. It is noteworthy that this influence is only discernible for diffusion coefficients in the stationary phase on the order of 10^{-5} cm^2 s^{-1} for the system examined here. For more typical values of the diffusion coefficient, on the order of 10^{-7} to 10^{-9} cm^2 s^{-1} [24–26], dispersion arising from the radial flow profile is negligible in comparison with that from kinetic contributions. Hence, it seems prudent to reevaluate the potential benefits to be gained by electrochromatography compared with traditional chromatography as well as the requisite conditions for their achievement [27].

4. Conclusions

From the stochastic simulation approach, a greatly improved understanding is derived of the kinetic processes involved in the partition mechanism. The diffusion-limited rate constants can be predicted via Eqs. (13a) and (13b) for any simple system consisting of a homogeneous fluid phase in contact with a homogeneous surface phase. In addition, the effect of these rate constants on the solute zone profile (mean, variance, and asymmetry) can be readily predicted. This simulation approach can now be applied to more complex separation mechanisms, such as partition or adsorption at multiple sites or a combined partition–adsorption mechanism. These types of studies are essential if the retention and dispersion processes inherent in complex chromatographic and electrophoretic systems are to be understood and controlled.

Appendix

The derivative of the characteristic time τ with respect to any variable x is obtained by applying the chain rule:

$$\frac{\partial \tau}{\partial x} = \frac{\partial \tau}{\partial k_{\mathrm{fs}}} \frac{\partial k_{\mathrm{fs}}}{\partial x} + \frac{\partial \tau}{\partial k_{\mathrm{sf}}} \frac{\partial k_{\mathrm{sf}}}{\partial x} \tag{A1}$$

From Eq. (14), it can easily be shown that the derivative of τ with respect to the individual rate constants k_{fs} and k_{sf} is given by

$$\frac{\partial \tau}{\partial k_{\mathrm{fs}}} = \frac{\partial \tau}{\partial k_{\mathrm{sf}}} = \frac{-1}{(k_{\mathrm{fs}} + k_{\mathrm{sf}})^2} = -\tau^2 \tag{A2}$$

By replacing x in Eq. (A1) with one of the system parameters from Eqs. (13a) and (13b), the effect of the parameter on the magnitude of τ can be evaluated. The resulting derivatives of the rate constants with respect to each of the system parameters are given below. For the equilibrium constant K:

$$\frac{\partial k_{\mathrm{fs}}}{\partial K} = \left(\frac{R_{\mathrm{f}}^2 (2R_{\mathrm{f}} R_{\mathrm{s}} + R_{\mathrm{s}}^2)}{[R_{\mathrm{f}}^2 + K(2R_{\mathrm{f}} R_{\mathrm{s}} + R_{\mathrm{s}}^2)]^2} \right) \left(\frac{1}{D_{\mathrm{f}}} + \frac{1}{D_{\mathrm{s}}} \right)^{-0.5}$$
$$\times \left(\frac{\pi R_{\mathrm{f}}}{D_{\mathrm{f}}} + \frac{\pi R_{\mathrm{s}}}{D_{\mathrm{s}}} \right)^{-0.5} \left(\frac{(R_{\mathrm{f}} + \pi R_{\mathrm{s}})^2}{R_{\mathrm{f}}^{1.5} R_{\mathrm{s}}^2} \right) \tag{A3a}$$

$$\frac{\partial k_{\mathrm{sf}}}{\partial K} = \left(\frac{- R_{\mathrm{f}}^2 (2R_{\mathrm{f}} R_{\mathrm{s}} + R_{\mathrm{s}}^2)}{[R_{\mathrm{f}}^2 + K(2R_{\mathrm{f}} R_{\mathrm{s}} + R_{\mathrm{s}}^2)]^2} \right) \left(\frac{1}{D_{\mathrm{f}}} + \frac{1}{D_{\mathrm{s}}} \right)^{-0.5}$$
$$\times \left(\frac{\pi R_{\mathrm{f}}}{D_{\mathrm{f}}} + \frac{\pi R_{\mathrm{s}}}{D_{\mathrm{s}}} \right)^{-0.5} \left(\frac{(R_{\mathrm{f}} + \pi R_{\mathrm{s}})^2}{R_{\mathrm{f}}^{1.5} R_{\mathrm{s}}^2} \right) \tag{A3b}$$

For the diffusion coefficient in the fluid phase D_{f}:

$$\frac{\partial k_{\mathrm{fs}}}{\partial D_{\mathrm{f}}} = \left(\frac{K(2R_{\mathrm{f}} R_{\mathrm{s}} + R_{\mathrm{s}}^2)}{R_{\mathrm{f}}^2 + K(2R_{\mathrm{f}} R_{\mathrm{s}} + R_{\mathrm{s}}^2)} \right)$$
$$\times \left(\frac{D_{\mathrm{s}}^2 [2\pi R_{\mathrm{f}} D_{\mathrm{s}} + \pi D_{\mathrm{f}}(R_{\mathrm{f}} + R_{\mathrm{s}})]}{2[(D_{\mathrm{f}} + D_{\mathrm{s}})(\pi R_{\mathrm{f}} D_{\mathrm{s}} + \pi R_{\mathrm{s}} D_{\mathrm{f}})]^{1.5}} \right)$$
$$\times \left(\frac{(R_{\mathrm{f}} + \pi R_{\mathrm{s}})^2}{R_{\mathrm{f}}^{1.5} R_{\mathrm{s}}^2} \right) \tag{A4a}$$

$$\frac{\partial k_{sf}}{\partial D_f} = \left(\frac{R_f^2}{R_f^2 + K(2R_fR_s + R_s^2)} \right)$$

$$\times \left(\frac{D_s^2[2\pi R_f D_s + \pi D_f(R_f + R_s)]}{2[(D_f + D_s)(\pi R_f D_s + \pi R_s D_f)]^{1.5}} \right)$$

$$\times \left(\frac{(R_f + \pi R_s)^2}{R_f^{1.5}R_s^2} \right) \tag{A4b}$$

For the diffusion coefficient in the surface phase D_s:

$$\frac{\partial k_{fs}}{\partial D_s} = \left(\frac{K(2R_fR_s + R_s^2)}{R_f^2 + K(2R_fR_s + R_s^2)} \right)$$

$$\times \left(\frac{D_f^2[2\pi R_s D_f + \pi D_s(R_f + R_s)]}{2[(D_f + D_s)(\pi R_f D_s + \pi R_s D_f)]^{1.5}} \right)$$

$$\times \left(\frac{(R_f + \pi R_s)^2}{R_f^{1.5}R_s^2} \right) \tag{A5a}$$

$$\frac{\partial k_{sf}}{\partial D_s} = \left(\frac{R_f^2}{R_f^2 + K(2R_fR_s + R_s^2)} \right)$$

$$\times \left(\frac{D_f^2[2\pi R_s D_f + \pi D_s(R_f + R_s)]}{2[(D_f + D_s)(\pi R_f D_s + \pi R_s D_f)]^{1.5}} \right)$$

$$\times \left(\frac{(R_f + \pi R_s)^2}{R_f^{1.5}R_s^2} \right) \tag{A5b}$$

For the radius of the fluid phase R_f:

$$\frac{\partial k_{fs}}{\partial R_f} = k_{fs} \left(-\frac{3}{2R_f} + \frac{2}{R_f + \pi R_s} + \frac{2\pi R_s}{2R_fR_s + R_s^2} \right.$$

$$\left. -\frac{2\pi(R_f + KR_s)}{R_f^2 + K(2R_fR_s + R_s^2)} - \frac{\pi D_s}{2\pi(R_f D_s + R_s D_f)} \right) \tag{A6a}$$

$$\frac{\partial k_{sf}}{\partial R_f} = k_{sf} \left(\frac{1}{2R_f} + \frac{2}{R_f + \pi R_s} \right.$$

$$\left. -\frac{2\pi(R_f + KR_s)}{R_f^2 + K(2R_fR_s + R_s^2)} - \frac{\pi D_s}{2\pi(R_f D_s + R_s D_f)} \right) \tag{A6b}$$

where k_{fs} and k_{sf} are given by Eqs. (13a) and (13b). For the radius of the surface phase R_s:

$$\frac{\partial k_{fs}}{\partial R_s} = k_{fs} \left(-\frac{2}{R_s} + \frac{2\pi}{R_f + \pi R_s} + \frac{2\pi(R_f + R_s)}{2R_fR_s + R_s^2} \right.$$

$$\left. -\frac{2\pi K(R_f + R_s)}{R_f^2 + K(2R_fR_s + R_s^2)} - \frac{\pi D_f}{2\pi(R_f D_s + R_s D_f)} \right) \tag{A7a}$$

$$\frac{\partial k_{fs}}{\partial R_s} = k_{sf} \left(-\frac{2}{R_s} + \frac{2\pi}{R_f + \pi R_s} \right.$$

$$\left. -\frac{2\pi K(R_f + R_s)}{R_f^2 + K(2R_fR_s + R_s^2)} - \frac{\pi D_f}{2\pi(R_f D_s + R_s D_f)} \right) \tag{A7b}$$

where k_{fs} and k_{sf} are given by Eqs. (13a) and (13b). Eqs. (A3a) and (A3b) through Eqs. (A7a) and (A7b) can be substituted into Eq. (A1) to obtain $\partial t / \partial x$, the slope of the graph of the characteristic time τ with respect to the chosen parameter.

References

[1] J.C. Giddings, J. Chromatogr. 2 (1959) 44.
[2] J.C. Giddings, J. Chem. Phys. 31 (1959) 1462.
[3] J.C. Giddings, J. Chromatogr. 3 (1960) 443.
[4] J.C. Giddings, J. Chromatogr. 5 (1961) 61.
[5] J.C. Giddings, Dynamics of Chromatography, Marcel Dekker, New York, NY, 1965.
[6] R.B. Bird, W.E. Stewart, E.N. Lightfoot, Transport Phenomena, Wiley, New York, NY, 1960.
[7] T.K. Sherwood, R.L. Pigford, C.R. Wilke, Mass Transfer, McGraw-Hill, New York, NY, 1975.
[8] A.L. Hines, R.N. Maddox, Mass Transfer: Fundamentals and Applications, Prentice-Hall, Englewood Cliffs, NJ, 1985.
[9] S. Golshan-Shirazi, G. Guiochon, in: F. Dondi, G. Guiochon (Eds.), Theoretical Advancement in Chromatography and Related Separation Techniques, Kluwer, Amsterdam, 1992, pp. 61–92.
[10] J.C. Giddings, H. Eyring, J. Phys. Chem. 59 (1955) 416.
[11] J.C. Giddings, J. Chem. Phys. 26 (1957) 169.
[12] D.A. McQuarrie, J. Chem. Phys. 38 (1963) 437.
[13] F. Dondi, M. Remelli, J. Phys. Chem. 90 (1986) 1885.
[14] C.P. Woodbury, J. Chromatogr. Sci. 32 (1994) 339.
[15] M.R. Schure, A.M. Lenhoff, Anal. Chem. 65 (1993) 3024.
[16] V.L. McGuffin, P. Wu, J. Chromatogr. A 722 (1996) 3.
[17] D.L. Hopkins, V.L. McGuffin, Anal. Chem. 70 (1998) 1066.
[18] W.H. Press, B.P. Flannery, S.A. Teukolsky, W.T. Vetterling, Numerical Recipes: The Art of Scientific Computing, Cambridge University Press, Cambridge, England, 1989.
[19] J.I. Steinfeld, J.S. Francisco, W.L. Hase, Chemical Kinetics and Dynamics, Prentice Hall, Englewood Cliffs, NJ, 1989.

[20] S.W. Benson, Foundations of Chemical Kinetics, McGraw-Hill, New York, NY, 1960.

[21] P. Wu, V.L. McGuffin, A.I.Ch.E. J. (1998) in press.

[22] H. Cramer, Mathematical Methods of Statistics, Princeton University Press, Princeton, NJ, 1946.

[23] E. Grushka, J. Phys. Chem. 76 (1972) 2586.

[24] R.G. Bogar, J.C. Thomas, J.B. Callis, Anal. Chem. 56 (1984) 1080.

[25] S.L. Zulli, J.M. Kovaleski, X.R. Zhu, J.M. Harris, M.J. Wirth, Anal. Chem. 66 (1994) 1708.

[26] R.L. Hansen, J.M. Harris, Anal. Chem. 67 (1995) 492.

[27] M.M. Robson, M.G. Cikalo, P. Myers, M.R. Euerby, K.D. Bartle, J. Microcolumn Sep. 9 (1997) 357.